Original paper

A new SOBP-formation method by superposing specially shaped Bragg curves formed by a mini-ridge filter for spot scanning in proton beam therapy

K. Yokokawa[a], M. Furusaka[b,c], T. Matsuura[c,d,e], S. Hirayama[f], K. Umegaki[c,d,e,*]

[a] Graduate School of Engineering, Hokkaido University, North-13 West-8, Kita-ku, Sapporo, Hokkaido 060-8628, Japan
[b] Faculty of Engineering, Hokkaido University, North-13 West-8, Kita-ku, Sapporo, Hokkaido 060-8628, Japan
[c] National Institute of Advanced Industrial Science and Technology, Tsukuba Central 2 1-1-1 Umezono, Tsukuba, Ibaraki Prefecture 305-8568, Japan
[d] Proton Beam Therapy Center, Hokkaido University Hospital, North-15, West-7, Kita-ku, Sapporo, Hokkaido 060-8628, Japan
[e] Global Station for Quantum Medical Science and Engineering, Global Institution for Collaborative Research and Education (GI-CoRE), Hokkaido University, Sapporo 060-8628, Japan
[f] Faculty of Medicine, Hokkaido University, North-15 West-7, Kita-ku, Sapporo, Hokkaido 060-8638, Japan

ABSTRACT

Purpose: We propose a new spread-out Bragg peak (SOBP) formation method for low-energy regions of spot-scanning proton therapy in order to reduce the required number of energy layers while maintaining high dose uniformity, while maintaining the distal falloff as sharp as possible.
Methods: We use only one specially shaped mini-ridge filter (MRF) to create new trapezoidal Bragg curves (TBCs) from very sharp pristine Bragg curves (PBCs) of low-energy proton beams. The TBC has three pre-designed dose regions of proximal, flat-top, and distal components. These components are designed to have nearly equal depth lengths and good linearity. Then, the required SOBP is formed by superposing the TBCs with the correct spacing and beam intensity weights. We then compare the performance of the TBC-based SOBPs with those formed by PBCs.
Results: The dose uniformities of the SOBP formed by the proposed method are kept within the design tolerance, and are equivalent to those of conventional SOBPs. The sharpness of the distal falloff is reasonably kept by the deepest TBC. The required number of energy layers is significantly reduced compared with that of conventional PBC-based SOBP.
Conclusions: The proposed method enables shortening of the irradiation time of spot-scanning proton beam therapy in low-energy regions with a reduced number of energy layers. It can be realized by using only one specially shaped MRF, which can be easily installed at any facility.

1. Introduction

The spot-scanning method enables delivery of highly conformal doses to target tumours while sparing surrounding healthy tissues. This is performed via lateral beam scanning and beam-energy adjustment [1,2].

Multiple Bragg curves with various incident energies are generally superposed using appropriate beam weights to form a spread-out Bragg peak (SOBP) with a specific length [3]. An important problem that should be addressed in the spot-scanning method is determining how to reduce the number of incident energy layers in the low-energy region. The energy spacing of the discrete layers becomes narrower as the

incident beam energy becomes lower in the low-energy region, because of the sharpness of the Bragg peaks. For instance, to form an SOBP with a high dose uniformity, the required energy spacing becomes 1 mm or 2 mm, which corresponds to the beam range spacing at the shallow region; approximately less than 100 mm from the surface of the body. Then, a large number of energy layers are required. In general, because the energy layer change requires a few seconds for the Synchrotron system operation, it is time-consuming and leads to a longer irradiation time. In addition, sharp Bragg peaks are extremely sensitive to range uncertainty in terms of the dose uniformity of the SOBP. Therefore, there is a need to effectively address this "sharp Bragg peak" problem in order to realize high-performance spot scanning in the low-energy

---

region.

To deal with this problem, a ridge filter (RF) or mini-ridge filter (MRF), which is a compensator used to broaden Bragg peaks, has been used in the conventional passive-scattering method [4] or scanning method [5]. The broadened peaks make it possible to reduce the number of energy layers required to form SOBPs [6,7]. However, the distal falloffs are also broadened simultaneously. In order to maintain sharp distal falloffs, a method using two types of MRF and their exchanger system has been proposed [8]. Based on this method, a special MRF that broadens the proximal region of the Bragg peak and keeps the sharpness of its distal region was used only for the deepest energy layer, and a normal MRF was used for the other layers. The efficiency of this method was successfully demonstrated. However, recently constructed spot-scanning systems have very compact nozzles, which are among the primary benefits of the scanning system, making it difficult to install multiple filters and their exchanger.

The main purpose of this study is to propose a new SOBP-formation method for spot-scanning proton beam therapy in the low-energy beam region to achieve the following objectives: reduce the required number of energy layers, keep the distal falloff as sharp as possible, maintain a reasonable dose uniformity, mitigate the dose error caused by range uncertainties, and realize an irradiation system that can be installed even at facilities that use a compact nozzle. To fulfil these conditions, we propose to use a specially shaped MRF to form an SOBP. The MRF produces modified Bragg curves named trapezoidal Bragg curves (TBCs). We are then able to form an SOBP that satisfies the aforementioned requirements simultaneously by superposing them. It is noteworthy that in this method, we use only one MRF in the low-energy region. In this paper, as a basic study, we clearly highlight the features of our proposed method compared to a conventional approach.

2. Materials and Methods

2.1. Conventional SOBP-formation method with pristine Bragg curves

In spot scanning irradiation method using proton beams, the therapeutic-energy region is normally chosen between 70 and 230 MeV. The beam range, R, and the Bragg-peak width are chosen according to the beam kinetic energy, E. Within the therapeutic-energy region, R varies from 40 mm to 300 mm in water-equivalent depth, and the Bragg-peak width becomes narrower as E becomes lower. In a conventional SOBP-formation method, multiple pristine Bragg curves (PBCs) with different E's are arranged with appropriate beam intensity weights and range-spacing to produce maximally uniform SOBP. General SOBP performance is represented by three main features listed as follows:

- **Dose uniformity:** The dose uniformity represents flatness of the generated depth-dose distribution within the SOBP-region. Even though the definitions of uniformity and SOBP-region are slightly different among different facilities, we set our design tolerance of uniformity to be within ± 2.5% [9] as a relative error from the target dose in the SOBP-region without 2 mm edges from both ends.
- **Distal-falloff sharpness:** The distal-falloff sharpness is defined as the depth-distance between 80% and 20% dose positions, $L_{80\text{-}20}$. The distance strongly depends on the sharpness and beam intensity weight of the PBCs, which influences the distal falloff of the SOBP. It becomes sharper as the range of SOBP becomes shallower.
- **The required number of energy layers:** The PBCs sequence for SOBP-formation is shown in Fig. 1 as a function of water-equivalent depth range. The beam range spacing d between adjacent PBCs is generally chosen from 1.0 mm to several millimetres in steps of 1.0 mm. Here, we defined them as 1.0 mm for R from 40 mm to 70 mm, 2.0 mm for R from 70 mm to 100 mm, and 3.0 mm for R from 100 mm to 130 mm, although the depth range arrangement varies slightly among facilities [10]. Note that the required number of energy
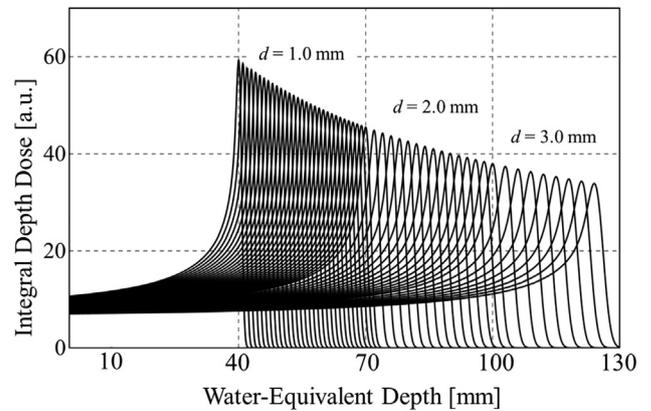

Fig. 1. The PBCs sequence for SOBP-formation based on range-spacing d as a function of water-equivalent depth range in the low-energy region.

layers becomes increasingly larger as the SOBP range becomes shallower. In this study, we regard the "low-energy region" as the depth range less than 100 mm where $d \leq 2.0$ mm.

2.2. Concept of SOBP-formation method with trapezoidal Bragg curves

2.2.1. Definition of trapezoidal Bragg curve (TBC)

In order to reduce the number of energy layers in the low-energy region, we propose to use a specially shaped composite Bragg curve, which we describe as a "trapezoidal Bragg curve (TBC)," formed by a specially designed mini-ridge filter (MRF). Fig. 2 shows an ideal shape of a TBC. The TBC is basically composed of multiple straight-line segments of equal depth interval l, throughout the curve. This parameter l determines the width of each part so that we henceforth represent TBC with l as TBCl (e.g. TBC3: $l = 3.0$ mm). The three segments at the deepest region denoted as A, B and C are regarded as the distal, flat-top, and proximal parts, which constitute the trapezoidal-like shape of the Bragg curve. The other segments denoted as D are collectively defined as the plateau region. We define the range R for TBCl as the deep end position of the flat-top part.

2.2.2. Procedure of SOBP-formation by superposing ideal TBCls

The method of forming an SOBP by superposing ideally shaped TBCls is described in the following section. Fig. 3 shows an example of a generated SOBP with the range, R_{SOBP}, and the length L_{SOBP}, by superposing several TBCls. In the first step, a TBCl with a range of R_{SOBP} is
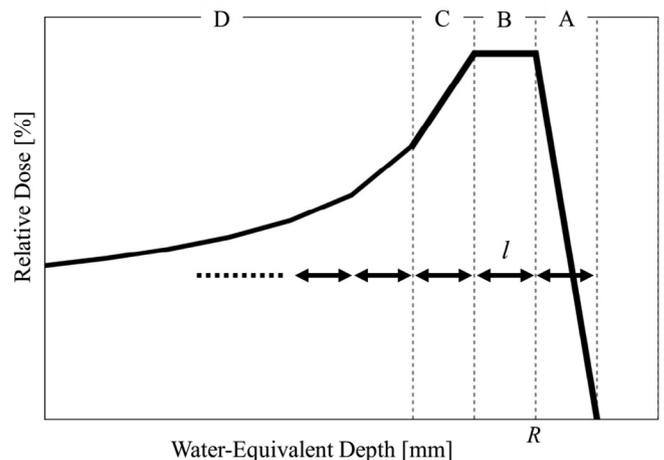

Fig. 2. Ideal shape of trapezoidal Bragg curve (TBC): distal part A; flat-top part B; proximal part C; and plateau region D. The parameters R and l represent the beam range and width of each part, respectively.
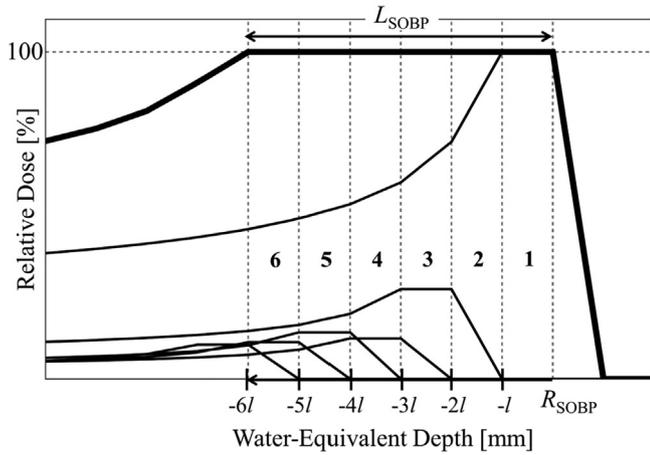
Fig. 3. Concept of SOBP-formation by superposing of several TBC*l*s. The thick solid line is the generated SOBP, and the thin solid lines are individual TBC*l*s. The range and length of the SOBP are represented by R_{SOBP} and L_{SOBP}. The numbers represent the order of superposition.

used to form the deepest region of the SOBP. In this case, the distal-falloff region and the deepest part of the flat-top with length *l* are formed solely by the deepest TBC*l*. In the next step, the second TBC*l* with the range of R_{SOBP}-2*l* is added by shifting 2*l* to a shallower position to extend the flat-top region. The beam intensity weight of the second TBC*l* is determined so that the slope of the distal part should have the same value with opposite sign to the first TBC*l*s proximal part to cancel out. Because of the linearity of the segments, the SOBP became flat at the overlapping region. Then, the third TBC*l* is added by shifting *l* to a shallower position from the second TBC*l* with an appropriate beam intensity weight. Here, the slope of the distal part of the third TBC*l* just compensates for the slope of the first TBC*l*s plateau region and the flat-top part of the second TBC*l* is added to them resulting in a flat part. The last procedure is repeated to extend the SOBP further by *l*. As a result, it is possible to form a uniform SOBP with $L_{SOBP} = nl$ (n is the number of TBC*l*).

2.2.3. Characteristics of SOBP formed by TBC*l*s
The basic characteristics of SOBP formed by TBC*l*s are as follows.

- **Dose uniformity:** Although it is possible to design the perfect flat-top region for an SOBP using ideally shaped TBC*l*s, the actual uniformity depends on the linearity of the TBC*l*s segments formed by the MRF. If non-linearity is well-controlled within a few errors, the uniformity can satisfy design tolerance. Moreover, superposition of TBC*l*s has the potential to reduce dose errors caused by range uncertainty errors compared with those of very sharp PBCs.
- **Distal-falloff sharpness:** the depth-distance L_{80-20} is basically controlled to be 0.6*l* because the distal-falloff region is formed solely by only one TBC*l*s distal part. Actually, the value varies slightly with a few factors such as the shaping accuracy of the distal part.
- **The required number of energy layers:** the required number of energy layers, N, for forming SOBP with an L_{SOBP} is expressed by L_{SOBP}/l. It is independent of the conventional beam range spacing *d* of PBCs. Thus the TBC*l*-based SOBP-formation can reduce the number to *d/l*.

2.3. Design of mini-ridge filter (MRF) for trapezoidal Bragg curve

2.3.1. Design condition for shaping MRF
Conventional filters such as ridge filters, mini-ridge filters, and ripple filters are designed to broaden a Bragg peak to a Gaussian-like shape. Typically, they have a one-dimensional repeated ridge-like structure; the investigation of two-dimensional periodic structures is in

progress [11,12]. Our objective is to obtain a desired trapezoidal Bragg curve shape using a practical MRF design.

Assuming a general isosceles triangle-like shaped MRF, the basic design parameters are represented by the maximum height T_{max}, base width λ (equal to the repeated interval length) and the actual shape of the triangle-like slope for a unit of the ridge structure. The parameter T_{max} corresponds to the desired width of the Bragg peak. To create the TBC*l*-shape, we need to set T_{max} up to 3*l* to control the shape of the distal, flat-top, and proximal parts. We utilized *l* = 3 mm in this study to simultaneously exploit both the advantages of using TBC*l*'s and the productivity of MRF with a reasonable height T_{max}. The parameter λ is determined by considering the lateral beam profile, influenced by the Gaussian beam size $\sigma_{lateral}$. Weber *et al.* (1999) showed that a proton beam that passes through the MRF can maintain a Gaussian profile in the case of λ ≤ 1.6$\sigma_{lateral}$ [13]. Although the size of $\sigma_{lateral}$ is different among the facilities, it is usually more than 5 mm within the low-energy region of interest in our facility. The minimum $\sigma_{lateral} = 4.0$ mm was determined by considering a margin and λ was then set to 6.4 mm. The shape of the slope was optimised to create the TBC*l* shape, where the limit of sharpness was set at the top of the ridge to enable manufacturing using a conventional method. We checked the actual gradients of some existing MRFs made of PMMA [13–15] and decided that the ratio of height to width less than 6 is adequate to fabricate practical MRFs. This ratio becomes approximately 7 (=6 × 1.165 [13]) when it is converted into a water equivalent thickness (WET).

2.3.2. Optimising the slope of MRF designed for TBC3
In the design of the actual MRF, it is necessary to define the range and the length, R_{SOBP} and length, L_{SOBP}, respectively, for the target SOBP. Then the required number of TBC*l*s and their ranges, *R*, are determined. Next, a PBC is selected to generate a corresponding TBC*l*. The PBC, which has a range R + *l*, is selected to shape the TBC*l* with a range R through the MRF. Here, 1 mm thickness was taken into account as a base of the MRF. The proton beam, which originally forms the PBC, reforms the three segment parts when they pass through the various heights in the MRF.

It should also be considered that only one MRF is designed to cover various SOBP-formations within a certain low-energy range. We also need to set an appropriate representative range, R_{MRF}, as a design point of the MRF to form TBC*l*s for a required energy range. It is necessary to confirm that the trapezoidal shape is sufficiently well-maintained within the required energy range by adopting an R_{MRF}-based design. To optimise the calculation of the slope-shape, the slope-shape was approximated by a fine step-structure. The height and width of the m-*th* step are represented by T_m and Δx_m, respectively. Here the T_m is expressed by WET and corresponds to the modulation range of the PBC that passes through the m-*th* step and Δx_m corresponds to the amount of partial dose. The step-height spacing resolution ΔT was set to 0.1 mm except for a 1 mm base part to accurately control the modulation range. We used the occupancy ratio $w_m = \Delta x_m /(\lambda/2)$ as a normalized value of the beam weight to optimize the calculation.

Here, we demonstrate the optimisation process of creating TBC3. The total number of steps, M is up to 90 for TBC3. Then the integral depth-dose distribution of TBC3, D_{TBC3} (z; E) can be analytically calculated using the following equation [8].

$$D_{TBC3} (z; E) = \sum_{m=1}^{M} w_m D_{PBC}(z + T_m; E)$$

$$\tag{1}$$

where E is the beam energy of the incident proton beam and D_{PBC} (z; E) is an integral depth-dose distribution of PBC given by an analytical formula [16]. The energy-spread $\Delta E/E$ was set to 0.4%, based on the results of Monte-Carlo simulation using Geant4.10.1 under the typical irradiation condition at our proton facility.

After setting the representative range $R_{MRF} = 40$ mm as a typical low energy range, which corresponds to 74.1 MeV incident energy, the

set of weights w_m's was optimised to generate a target shape for TBC3. We defined the objective function using a sequence of points on the trapezoidal shape with 0.2 mm for the proximal, flat-top, and distal parts. Points on both corners of the flat-top part and the end of the distal part were excluded. The constraint condition was set for w_m combination such that the amplitude of w_m change next to each other should remain within a certain range to create a continuous profile of w_m sets. This is because the trapezoidal shapes are properly maintained within the target range region even when one MRF design with R_{MRF} is used, by maintaining the appropriate MRF balance of each w_m contribution as the beam weight.

In the calculation process, we examined whether the required ratio of height to width is satisfied when the value is less than 7, or not in the top region of the MRF. If the ratio is more than 7, the top of the ridge is cut, and the height is reduced and a set of w_m is recalculated until the ratio becomes less than 7. Finally, we obtained the most effective T_{max} and the optimized set of w_m which can satisfy both the design constraint and the appropriate TBC3 shape. All calculations were conducted using Wolfram's Mathematica ver. 10.2 software. After the optimization calculation, all the T_ms were divided by 1.165 to convert the height scale to the thickness of the MRFs made of PMMA.

Fig. 4(a) shows the schematic cross-sectional view of the optimized MRF shape for TBC3. The T_{max} in the scale of the PMMA thickness is 6.4 mm, which corresponds to 7.5 mm in the WET scale. The T_{max} was less than $3l = 9$ mm in the WET scale to satisfy the constraint of the height to width ratio. Fig. 4(b) shows the result of the relative dose distribution of TBC3 calculated using the analytical Eq. (1) and the target shape of TBC3. It is confirmed that the shape of TBC3 is reasonably for fitting to the target shape.

2.3.3. Verification of optimisation calculation by Monte-Carlo simulation

In order to verify the result of the optimisation calculation using the analytical equation, we also calculated the dose distribution using a designed MRF as shown in Fig. 4(a) using the Monte-Carlo simulation code, Geant4.10.1. We set the appropriate geometry for the irradiation nozzle for the designed MRF to realize the equal condition for analytical calculation. The incident beam energy was set to 74.1 MeV to have a beam range of $R + l = 43$ mm. Fig. 5 shows the result of the calculated TBC3 with $R = 40$ mm. The solid line and circle markers show the calculated $D_{TBC3}(z; E)$ obtained using the analytical equation and Monte-Carlo code, respectively. The results are in agreement and it was confirmed that the optimisation calculation using the analytical equation is sufficiently reliable for TBC3 design.
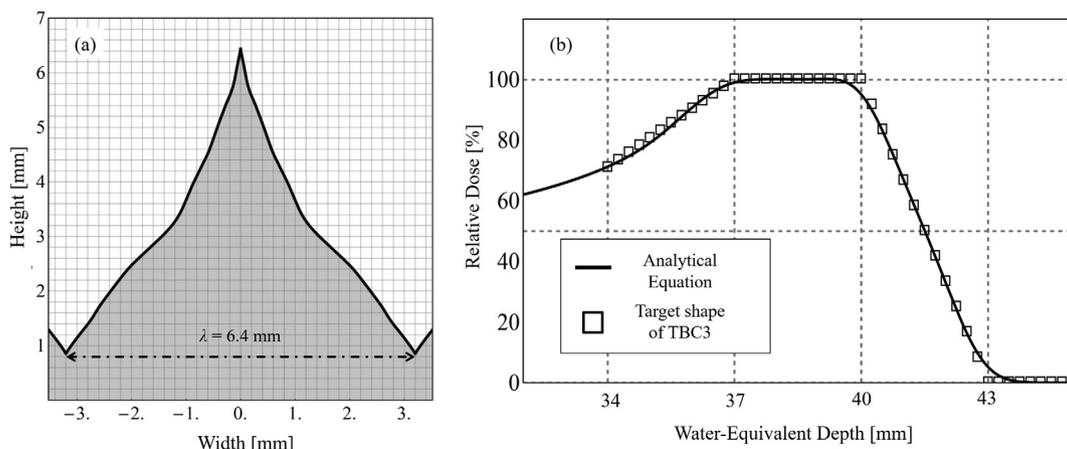

Fig. 5. Depth-dose distribution of calculated TBC3 with $R = 40$ mm. The thick and solid line and white circle markers show the calculated $D_{TBC3}(z; E)$ using the analytical formula and Monte-Carlo simulation, respectively. The thin and solid line and black circle markers show the calculated $D_{PBC}(z; E)$ using the analytical formula and Monte-Carlo simulation, respectively.

3. Results

3.1. Evaluation conditions of actual SOBP-formation

We evaluated the performance of the proposed SOBP-formation method using TBC3 as a proper reference. To evaluate the actual performance, three types of SOBPs with a range of R_{SOBP} and a length of L_{SOBP} were used: (a) $R_{SOBP} = 55$ mm and $L_{SOBP} = 15$ mm (depth between 40 mm and 55 mm), (b) $R_{SOBP} = 70$ mm and $L_{SOBP} = 30$ mm (depth between 40 mm and 70 mm), and (c) $R_{SOBP} = 100$ mm and $L_{SOBP} = 60$ mm (depth between 40 and 100 mm). Using the TBC3s, SOBPs in the depth range from 40 mm to 100 mm was formed to satisfy the relationship $d < l$.

The performance, such as the dose uniformity, sharpness of the distal-falloff (L_{80-20}) and the required number of energy layers, N, of the SOBP formed by TBC3s were compared with those of conventional SOBPs formed by PBCs. In the evaluation, the dose uniformity, DU, is defined by Eq. (2), as a relative dose error from the target dose.

$$DU = \frac{d_{max} - d_{min}}{d_{max} + d_{min}} \times 100[\%], \tag{2}$$

where d_{max} and d_{min} are the maximum and minimum dose within the SOBP-region, respectively. We evaluated DU to determine whether to maintain this parameter to within ± 2.5% error or not in the effective SOBP-region.

Fig. 4. (a) Schematic cross-sectional view of MRF designed for $D_{TBC3}(z; E)$: (b) Depth-dose distribution of calculated TBC3 with $R = 40$ mm. In Fig. 4(b), the solid line shows $D_{TBC3}(z; E)$ calculated using the analytical formula and the square markers show the target shape of the TBC3.
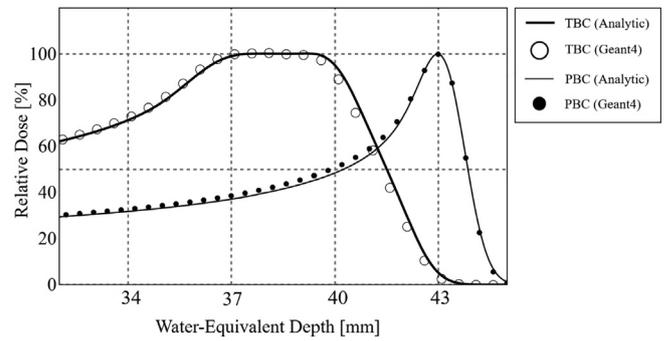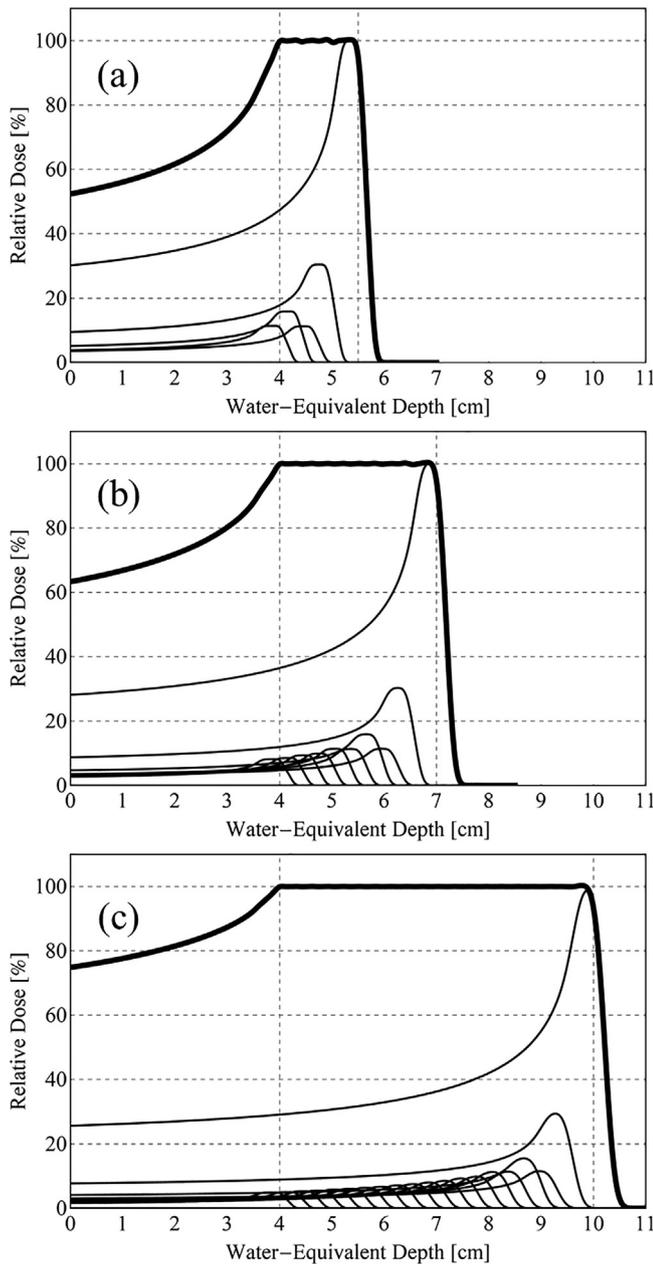
Fig. 6. Generated SOBPs using TBC3s: (a) $R_{SOBP} = 55$ mm and $L_{SOBP} = 15$ mm; (b) $R_{SOBP} = 70$ mm and $L_{SOBP} = 30$ mm; and (c) $R_{SOBP} = 100$ mm and $L_{SOBP} = 60$ mm.

3.2. Evaluation of SOBP performances

Fig. 6 shows the generated SOBPs formed using TBC3s with (a) $R_{SOBP} = 55$ mm and $L_{SOBP} = 15$ mm, (b) $R_{SOBP} = 70$ mm and $L_{SOBP} = 30$ mm, and (c) $R_{SOBP} = 100$ mm and $L_{SOBP} = 60$ mm. Table 1 shows the three characteristics of the generated of SOBPs, Dose uniformity, Distal-falloff Sharpness, and the Required Number of Energy Layers when TBC3s are used.

- **Dose uniformity:** The overall results show that the dose uniformities improve as R_{SOBP} and L_{SOBP} become larger. However, the uniformities for all cases were satisfactory ($\leq 2.5\%$). These variations are caused by the actual quality of the shape of the TBC3s.
- **Distal-falloff sharpness:** The $L_{80\text{-}20}$s of the TBC3 were between 1.32 and 1.73 times larger than those of the PBCs. These absolute differences are less than 1.0 mm in all cases. In addition, the

Table 1
Characteristics of generated SOBPs formed using TBC3s or PBCs. DU = Dose Uniformity, $L_{80\text{-}20}$ = Distal-falloff sharpness, N = The required number of energy layers.

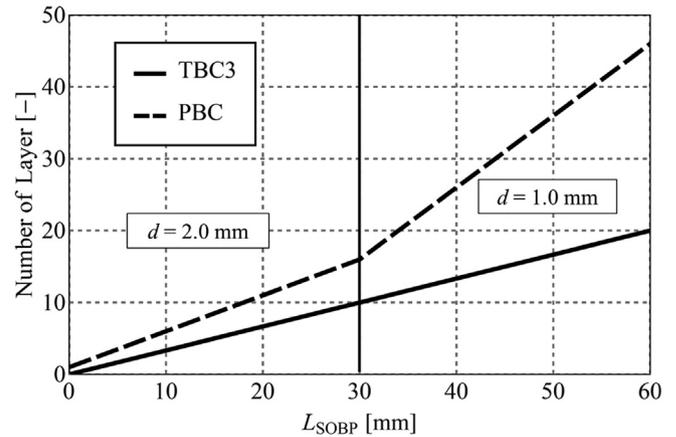| R_{SOBP}/L_{SOBP}	TBC3			PBC		
	DU	$L_{80\text{-}20}$	N	DU	$L_{80\text{-}20}$	N
55/15 mm	0.45	1.9	5	0.11	1.1	16
70/30 mm	0.31	2.1	10	0.06	1.3	31
100/60 mm	0.18	2.5	20	0.19	1.9	46

Fig. 7. Comparison of the required number of energy layers for SOBP-formation between PBC and TBC3s. The solid and dashed lines show the TBC3 and PBC cases, respectively.

theoretical value of $0.6\,l$ of TBC3 is 1.80 mm. However, all $L_{80\text{-}20}$s of the TBC3s were slightly larger. The slight change from the theoretical value of $L_{80\text{-}20}$ is primarily due to the broadening Bragg-peak width with increasing kinetic energy of incident proton beams.
- **The required number of energy layers:** In terms of the required number of energy layers, the use of TBC3s could greatly reduce this number when compared to using PBCs according to the ratio of d/l. Fig. 7 shows a comparison of the number of energy layers between the SOBPs formed by the TBC3s and those formed by PBCs. In this case, the range of the SOBP (R_{SOBP}) was assumed to be 100 mm. The horizontal axis represents the SOBP length (L_{SOBP}) starting from R_{SOBP}. For example, 30 mm indicates 30 mm of SOBP length starting at a depth of 100 mm and ending at 70 mm in Fig. 7. In the process of making a SOBP with an initial depth of 100 mm, the range-spacing d for the PBCs (as shown in Fig. 1) is 2 mm, and l for TBC3 is 3 mm. Thus, in this case, the N becomes 1.5 times the region between 0 mm and 30 mm length in Fig. 7. If the length is extended from 30 mm to 60 mm, l for TBC3 remains constant at 3 mm, but in the case of the PBCs, d changes to 1 mm. Thus, N triples in magnitude starting from 30 mm up to the 60 mm region. Altogether, if it is counted from 0 mm to 60 mm, N for TBC3 is reduced to approximately 4/9 of the PBC case. These differences appeared in the region of $d \leq l$ and becomes pronounced as the SOBP length increases.

4. Discussion

In this chapter, we discuss the SOBP performance variation when choosing the different representative range, R_{MRF} for TBCl. The target range of R_{SOBP} is from 40 mm to 100 mm, and we chose $R_{MRF} = 40$ mm to generate TBC3. The performance of SOBP such as the dose uniformity and the distal-falloff sharpness was varied by shifting R_{MRF}. Here, we additionally evaluated the SOBP performance for $R_{MRF} = 70$ mm for reference.

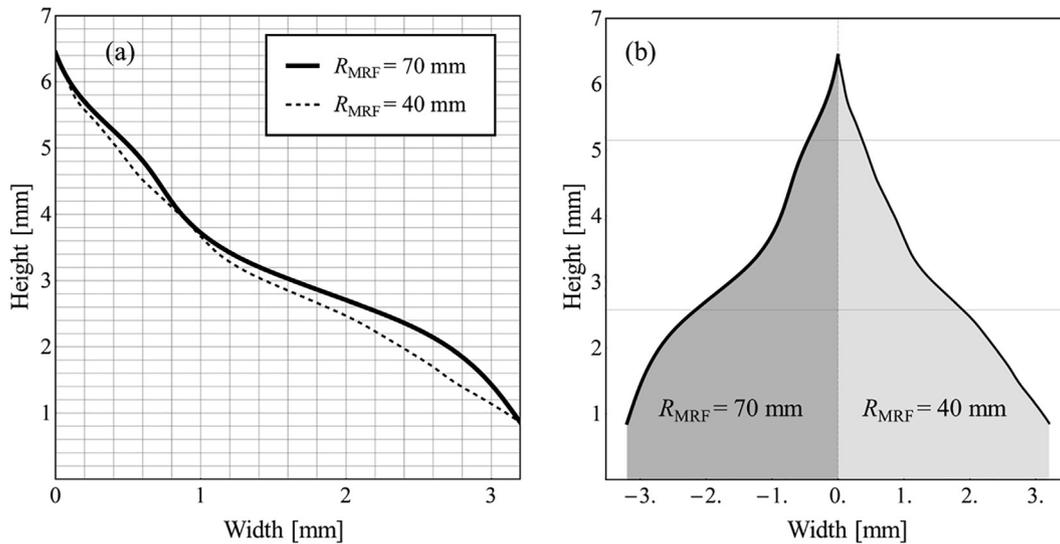Fig. 8(a) and (b) show a comparison of the optimised slope structure

Fig. 8. (a) Comparison of slope-structure of MRFs for $R_{MRF} = 70$ mm (solid line) and $R_{MRF} = 40$ mm (dashed line). The display range is from 0 to $\lambda/2$: (b) Schematic cross-sectional view in real scale of MRFs for $R_{MRF} = 70$ mm (left) and for $R_{MRF} = 40$ mm (right).
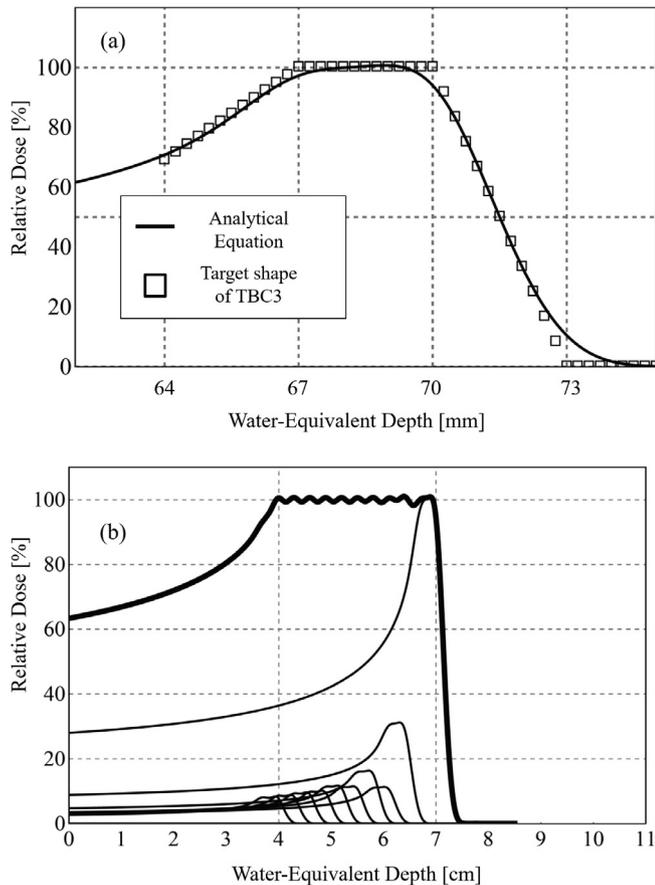

Fig. 9. (a) TBC3 with $R_{MRF} = 70$ mm. The solid line shows the $D_{TBC3}(z; E)$ calculated using the analytical formula and the square markers represent a target shape: (b) An SOBP with $R_{SOBP} = 70$ mm and $L_{SOBP} = 30$ mm in the case of $R_{MRF} = 70$ mm.

of the MRFs for $R_{MRF} = 70$ mm (solid line) and 40 mm (dashed line). The slope of the MRF for $R_{MRF} = 70$ mm became slightly undulated compared with that for $R_{MRF} = 40$ mm. Both slopes maintain the constraint that the height to width ratio is less than 6 in the top region. Fig. 9(a) shows the optimized TBC3 with $R = 70$ mm. The curve

calculated using the analytical formula could reasonably trace the target shape of TBC3. Fig. 9(b) shows the SOBP with $R_{SOBP} = 70$ mm and $L_{SOBP} = 30$ mm for the case of $R_{MRF} = 70$ mm. Compared to the case of $R_{MRF} = 40$ mm, dose uniformity DU slightly deteriorates to 1.4%, however, the distal-falloff sharpness L_{80-20} is improved to 1.9 mm. A sharper L_{80-20} is obtained because if the R_{MRF} value is chosen to be close to R_{SOBP}, the distal-falloff of SOBP is mainly represented by the distal part of TBC3 with R_{MRF}. The degradation of DU occurs because the deformations of TBC3 with $R < R_{MRF}$ is slightly larger than that of TBC3 with $R > R_{MRF}$. These results indicate that there is a trade-off relationship between dose uniformity and distal-falloff sharpness that is influenced by the R_{MRF} choice. Therefore, an appropriate R_{MRF} should be chosen according to treatment requests and/or irradiation conditions.

5. Conclusion

Bragg curves become very sharp when low-energy proton beams are used for spot scanning. As a result, the required number of energy layers to form the SOBP becomes larger, and the dose uniformity is more sensitive to range uncertainties. It is difficult to address these problems while maintaining a high dose uniformity and sharp distal-falloff. To resolve these conflicting issues, we developed a new SOBP-formation method by superposing specially shaped trapezoidal Bragg curves (TBCs). The TBC has three pre-designed dose regions of the front, increasing 'proximal part', constant 'flat-top part', and the rear decreasing 'distal part', which were formed such that they have almost equal depth lengths and good linearity. The TBCs are created using a specially designed mini-ridge filter (MRF) for the low-energy region. In order to verify the advantages of the TBCs, the characteristics of typical SOBPs were compared with those formed by pristine Bragg curves (PBCs). The proposed method enables a significant reduction in the number of energy layers for SOBP formation. In addition, it simultaneously facilitates good dose uniformity and a reasonably sharp distal-falloff. The reduced number of energy layers leads to a shorter irradiation time and higher efficiency of the treatment time. The system is sufficiently simple to allow installation at any facility because the method requires only one appropriately designed MRF in the low energy region.

Acknowledgement

References

[1] Kanai T, Kawachi K, Kumamoto Y, Ogawa H, Yamada T, Matsuzawa H, et al. Spot scanning system for proton radiotherapy. Med Phys 1980;7(4):365–9.

[2] Lomax A, et al. Treatment planning and verification of proton therapy using spot scanning: initial experiences. Med Phys 2004;31(11):3150–7.

[3] Jette D, Chen W. Creating a spread-out Bragg peak in proton beams. Phys Med Biol 2011;56:N131–8.

[4] Akagi T, Higashi A, Tsugami H, Sakamoto H, Masuda Y, Hishikawa Y. Ridge filter design for proton therapy at Hyogo Ion Beam Medical Center. Phys Med Biol 2003;48:N301–12.

[5] Matsuura T, et al. Development and evaluation of a short-range applicator for treating superficial moving tumors with respiratory-gated spot-scanning proton therapy using real-time image guidance. Phys Med Biol 2016;61:1515–31.

[6] Courneyea L, Beltran C, Tseung H, Yu J, Herman M. Optimizing mini-ridge filter thickness to reduce proton treatment times in a spot-scanning synchrotron system. Med Phys 2014;41:061713.

[7] Xianliang W, et al. Synchrotron-based pencil beam scanning nozzle with an integrated mini-ridge filter: a dosimetric study to optimize treatment delivery. Cancers 2017;9:170.

[8] Fujitaka S, Takayanagi T, Fujimoto R, Fujii Y, Nishiuchi H, Ebina F, et al. Reduction of the number of stacking layers in proton uniform scanning. Phys Med Biol 2009;54:3101–11.

[9] Farr JB, Mascia AE, His WC, Allgower CE, Jesseph F, Schreuder AN, et al. Clinical characterization of a proton beam continuous uniform scanning system with dose layer stacking. Med Phys 2008;35(11):4945–54.

[10] Zhu X, Poenisch F, Li H, Zhang X, Sahoo N, Gillin M. Field Shaping: Scanning Beam. In: Das I.J., Paganetti H. (Eds.), Principles and Practice of Proton Beam Therapy, AAPM Monograph No.37; 2015.

[11] Ringbæk T, Weber U, Peterson J, Thomsen B, Bassler N. Monte Carlo simulations of new 2D ripple filters for particle therapy facilities. Acta Oncol 2014;53(1):40–9.

[12] Tansho R, Furukawa T, Hara Y, Mizushima K, Saotome N, Saraya Y, et al. Development of a new ridge filter with honeycomb geometry for a pencil beam scanning system in particle radiotherapy. Nucl Phys B 2017;406:352–5.

[13] Weber U, Kraft G. Design and construction of a ripple filter for a smoothed depth dose distribution in conformal particle therapy. Phys Med Biol 1999;44:2765–75.

[14] Bourhaleb F, et al. Monte Carlo simulations of ripple filters designed for proton and carbon ion beams in hadrontherapy with active scanning technique. J Phys Conf Ser 2008;102:012002.

[15] Yang ZX, Zhang MZ, Li DM. Optimization of ripple filter for pencil beam scanning. Nucl Sci Tech 2013;24:060404.

[16] Bortfeld T. An analytical approximation of the Bragg curve for therapeutic proton beams. Med Phys 1997;24:2024–33.